Published in final edited form as:
J Neurosci. 2009 April 8; 29(14): 4675–4680. doi:10.1523/JNEUROSCI.5294-08.2009.

Uniform signal redundancy of parasol and midget ganglion cells in primate retina

Jeffrey L. Gauthier[1,†], **Greg D. Field**[1,†], **Alexander Sher**[2], **Jonathon Shlens**[1], **Martin Greschner**[1], **Alan M. Litke**[2], and **E.J. Chichilnisky**[1]

[1]Salk Institute for Biological Studies, La Jolla, CA

[2]Santa Cruz Institute for Particle Physics, University of California, Santa Cruz, CA

Abstract

The collective representation of visual space in high resolution visual pathways was explored by simultaneously measuring the receptive fields of hundreds of ON and OFF midget and parasol ganglion cells in isolated primate retina. As expected, the receptive fields of all four cell types formed regular mosaics uniformly tiling the visual scene. Surprisingly, comparison of all four mosaics revealed that the overlap of neighboring receptive fields was nearly identical, for both the excitatory center and inhibitory surround components of the receptive field. These observations contrast sharply with the large differences in the dendritic overlap between the parasol and midget cell populations, revealing an unexpected relationship between the anatomical and functional architecture in the dominant circuits of the primate retina.

Introduction

Populations of sensory neurons encode information collectively, and a fundamental aspect of the population code is *signal redundancy*, n. the degree to which features of sensory space are represented by more than one neuron. In the mammalian retina, roughly 20 types of retinal ganglion cells (RGCs) sample visual space [11, 48], and each cell type forms a lattice of regularly spaced receptive fields (RFs) that overlap their neighbors in the lattice to a greater or lesser degree [32, 16, 43, 41]. Greater RF overlap implies greater signal redundancy in the neural encoding [41, 38], which may be valuable for downstream computations that are sensitive to noise, but could also produce a less efficient neural representation. In the primate visual system, anatomical and physiological studies have yielded conflicting predictions about the degree of signal redundancy in the magnocellular and parvocellular pathways, which provide the highest resolution visual signals to the brain and are a major focus of current research.

Anatomical findings suggest a substantial difference in the signal redundancy of parasol and midget retinal ganglion cells [37, 46] which form the dominant input to the magnocellular and parvocellular pathways, respectively [28, 35, 36, 12]. The dendritic fields (DFs) of parasol cells overlap extensively, while midget cell DFs exhibit no overlap [12, 14, 10], as depicted in Figure 1A. If the RFs of these populations exhibited a correspondingly large difference in overlap, parasol cells would sample the visual scene with high signal redundancy, while midget cells would provide more independent samples, perhaps reflecting their distinct roles in visual function [30].

Contact: E.J. Chichilnisky, Systems Neurobiology, The Salk Institute, 10010 North Torrey Pines Road, La Jolla, CA 92037, USA. ej@salk.edu, phone: (858) 453-4100.
[†]these authors contributed equally

A conflicting prediction arises from physiological measurements in rabbit retina. One study [16] revealed nearly identical RF overlap in a variety of different ganglion cell types (see also [4]; but see [43]). This finding suggests that a single degree of signal redundancy can satisfy a range of visual processing requirements. In principle, parasol and midget cells could also exhibit a common degree of signal redundancy, despite their substantial anatomical differences and apparently different roles in vision. Although the RF structure of individual parasol and midget cells has been examined previously ([9], see [25]), the RF overlap of these important RGC populations has not.

We examined the collective representation of visual space in populations of parasol and midget ganglion cells by applying large-scale electrophysiological recordings to isolated peripheral primate retina [29, 21]. Within the regular mosaic formed by each cell type, ON and OFF midget and parasol cells exhibited nearly identical RF overlap, in both the center and surround components of the RF. Thus, retinal circuitry precisely compensates for striking differences in anatomical structure, producing a common functional organization in the parvocellular and magnocellular pathways.

Methods

Preparation and Recording

Retinas were obtained and recorded as described previously [8, 20]. Briefly, eyes were enucleated from terminally anesthetized macaque monkeys (*Macaca mulatta*) from a variety of sources (see [20]) in accordance with institutional guidelines for the care and use of animals. Immediately after enucleation, the anterior portion of the eye and vitreous were removed in room light. Following a dark incubation period, patches of peripheral retina were isolated from the pigment epithelium and placed flat, RGC layer down, on a planar array of 512 extracellular microelectrodes covering an area 1890 μm × 900 μm. During recording, the retina was kept at 33–35°C and was perfused with Ames' solution bubbled with 95% O_2 and 5% CO_2, pH 7.4.

Raw voltage recordings were analyzed offline to isolate the spikes of single cells, as described previously [20]. Briefly, candidate spike events were detected using a threshold on each electrode, and the voltage waveform on the center and nearby electrodes in the vicinity of spike events was saved. Spikes were clustered based on waveform shape, and spike clusters were identified as candidate neurons if they exhibited a refractory period and an average spike rate >1 Hz. Duplicate recordings of the same cell were identified by temporal cross-correlation and removed.

RF Characterization

RFs were mapped as described previously [8, 20]. Briefly, the optically reduced image of a gamma-corrected cathode ray tube computer display (Sony Multiscan E100) refreshing at 120 Hz was focused on the photoreceptor outer segments, and low photopic intensity was achieved by neutral density filters in the light path. A white noise stimulus was presented, consisting of a lattice of squares, each flickering randomly and independently at 30 or 120 Hz [7], with the intensities of the red, green, and blue display phosphors within each square varying independently. The contrast of this stimulus for each of the three display phosphors was 96% (SD of modulation divided by mean intensity), and the sidelengths of individual squares (henceforth, pixels) varied from 30 μm to 60 μm. The RF of each recorded cell was mapped by computing the spike triggered average (STA) stimulus during the white noise presentation (see [39, 7]).

RFs were summarized by fitting with a parametric model. The model consisted of the product of three profiles: spatial, temporal, and chromatic [8]. The temporal profile was a

difference of lowpass filters. The spatial profile consisted of a difference of 2-dimensional elliptical Gaussian functions. The chromatic profile was the relative weighting of the three monitor phosphors. Surrounds were relatively weak, so the cell surrounds could not be fitted individually in a robust fashion. However, on average, the STA spatial profile was well described by a fit in which the radius of the surround was twice that of the center. Thus, the following procedure was used to fit the spatial profile. A single two-dimensional Gaussian was fitted to the STA of each cell, generating a rough estimate of receptive field center location and radius. An inhibitory surround was then introduced, and the fit was re-optimized over all remaining parameters, with the surround radius constrained to be twice the center radius. Several parameters of the fit were extracted to visualize RF extent: the location of the Gaussian fit center, the SDs along the major and minor axes, and the angle of the major axis. These parameters defined an ellipse for each cell that represented the 1 SD contour of the Gaussian fit. In figures, receptive field outlines are represented using this contour.

Cell Type Classification and Identification

The anatomical cell type of recorded cells was determined using a two step procedure, as described previously [8, 20]. Briefly, cells were first grouped into functional cell classes based on their light response properties. Correspondences between functional classes and anatomical types were determined by density and light response properties. This procedure definitively identified the ON and OFF parasol and midget cells in each recording.

Coverage

Anatomical coverage of dendritic fields is usually defined as the average number of cells sampling any given point in visual space. In the case of receptive fields approximated by Gaussian fits, the extent is not well defined. Instead, receptive field overlap was analyzed using the normalized nearest neighbor distance (NNND). For a given cell, the NNND is given by $2R/(\sigma_1 + \sigma_2)$, where R is the distance between the Gaussian fit center points of each cell and its nearest neighbor in the mosaic, and σ_1, σ_2 are SDs of the fits measured along the line connecting the center points. Thus, for nearest neighbors that exactly touch at the 1 SD boundary, the NNND is 2. Note that the NNND is large when overlap is small, and vice-versa. This representation has the advantages of being closely related to a standard anatomical measure (NND) and allowing for unbiased comparison of overlap in cell types with different absolute sizes.

A control analysis verified that the estimate of the NNND was not affected by different pixel sizes. In one preparation, RFs were measured using several pixel sizes (96, 60, and 18 μm per pixel), and the NNND was computed for the ON and OFF parasol cells and ON midget cells. Within each cell type, the modal NNND value varied by less than 12% across the three pixel sizes, demonstrating that pixel size did not significantly affect the NNND.

RF Profiles

The average RF profile of neighboring cells was computed separately for each mosaic in several steps. First, the spatial part of the RF was obtained by applying singular value decomposition to STA frames where the contrast intensity was at least 20% of the peak contrast. These were usually the frames approximately 80 to 30 milliseconds before the spike. Second, the center point of each spatial RF was estimated by taking the center of mass of all pixels with amplitude at least half that of the highest amplitude pixel. Third, the amplitude of each STA was scaled so that the central region of the STA had unit variance. The central region was the circle centered on the center of mass with a radius of 3 times the nearest neighbor spacing. Fourth, the line connecting each cell to its nearest neighbor was computed. Along this line, absolute distance was normalized so that the nearest neighbor

was exactly 1 unit away. Fifth, the RF amplitude of the reference cell and its nearest neighbor at each pixel along the nearest neighbor line were extracted. Thus the RF intensity was a continuously valued function with a staircase shape representing the distinct pixels in the RF. Finally, the RF profiles were averaged for each reference cell. The amplitude was normalized so that the variance over the range shown in Figure 3 had unit variance.

Results

Receptive field mosaics of parasol and midget cells

Light responses of hundreds of retinal ganglion cells were simultaneously recorded in isolated segments of macaque monkey retina. The receptive field (RF) of each cell was identified using reverse correlation with a white noise stimulus [8]. Cells were functionally classified as ON and OFF parasol and midget based on their light response properties and density [20]. To visualize RFs, the center component was extracted from a difference of Gaussians fit to the spatial sensitivity profile (see Methods; [40]). The RF center boundary was represented graphically by the 1 SD contour of the Gaussian fit [16]. This definition of the RF spatial extent, though arbitrary, permits a standardized comparison between RFs of different cell types. Figure 1B,C shows the RF centers of simultaneously recorded ON and OFF parasol and midget cells from two preparations. As expected from previous work [12, 10, 8, 21, 20], the RFs of each cell type formed a regularly spaced lattice, or mosaic. The observed mosaic structure indicates that, over some regions of retina, all or nearly all cells of each type were recorded. This complete sampling is essential for reliably measuring the signal redundancy in each cell type.

Overlap of neighboring receptive field centers

Visual inspection of Figure 1B,C suggests that parasol and midget RFs exhibit similar RF overlap: the RFs of all four cell types appear to abut their neighbors at approximately the 1 SD boundary shown by the outlines. Note that this does not imply no overlap of RFs: a substantial fraction of the RF lies outside the 1 SD boundary. However, the similar pattern across cell types suggests equal overlap.

This suggestion was confirmed quantitatively by measuring the spacing of cells in each mosaic, relative to the size of the RFs. The distance between neighboring RF centers was divided by the equivalent RF radius, producing a normalized nearest neighbor distance (NNND; see Methods, [16]). For a mosaic with high (low) overlap, the NNND will be small (large). When neighboring RFs just touch at the 1 SD boundary, the NNND value is 2. Figure 2A shows the NNNDs for each cell type from the preparation of Figure 1B. The modal NNND of each cell type is represented graphically beneath the abscissa. For all four cell types, the modal NNND was near 2, confirming the impression that the RFs of neighboring cells abut roughly at the 1 SD outline. Figure 2B shows similar results for the preparation of Figure 1C.

Parasol and midget cells exhibited nearly identical RF overlap in multiple recordings over a range of eccentricities. Figure 2C shows modal NNNDs of parasol and midget cells, summarizing the RF overlap of 36 mosaics (3,221 cells spanning 10 retinas). ON and OFF populations are represented by open and closed circles, respectively. The data fall near the identity line (solid line) that indicates equal RF overlap. This finding contrasts with the approximately two-fold difference predicted from DF overlap (dashed line). On average, ON cells exhibited slightly more overlap than OFF cells, for both parasol and midget populations [8]. Figure 2D reveals that overlap did not vary with retinal eccentricity across the peripheral visual field. Over the range of eccentricities recorded, RF sizes varied by

roughly two-fold. Thus, the observed overlap is a consistent feature that is independent of absolute RF size.

Overlap of neighboring receptive field profiles

The above results were confirmed over the entire extent of the RF, including the inhibitory surround, by directly examining light sensitivity profiles. For each reference cell, light sensitivity was measured along the line connecting the RF center to that of the nearest neighbor in the mosaic, producing two spatial profiles: one for the reference cell, and one for the neighbor. The reference and neighbor profiles were averaged across every reference cell in the mosaic. These profiles were normalized to focus on profile shape independently of absolute size, spacing, and sensitivity (see Methods).

Figure 3A shows the resulting average neighbor profiles for ON and OFF parasol and midget cells from the preparation of Figure 1C. All four cell types exhibited nearly identical overlap in neighbor profiles, though the ON parasol cells exhibited a slightly flatter peak, and, as in Figure 2C, ON cells exhibited slightly greater overlap. The closely overlaying profiles confirm that RF overlap is nearly equal in all four cell types. Unlike the parametric analysis above, this analysis also shows the contribution of the inhibitory RF surrounds, which overlay closely. Similar results were observed in a second preparation (Figure 3B).

Discussion

ON and OFF parasol and midget cells exhibited nearly identical RF profiles and overlap in the conditions examined. This implies that retinal circuitry precisely counteracts substantial differences in the anatomical structure of these populations, producing a highly uniform functional organization in the magnocellular and parvocellular visual pathways.

Functional vs. anatomical overlap

The striking discrepancy between structure and function distinguishes the present study from previous work on RGC populations for which less anatomical information is available [16, 4, 43, 41] (see below). Parasol cell DFs overlap substantially, while midget cell DFs overlap little or not at all [12, 14, 10] (see Figure 1A). Therefore, the present results imply that the relationship between RF and DF is not universal, but is unique to each cell type. This fact presumably reflects the diversity of the bipolar and amacrine cell circuits contacting each RGC type (see [18]), an issue that has been raised but not resolved in previous studies of the relation between RF and DF structure [33, 34, 49, 5]. For example, the relatively larger size of bipolar cell RFs in the midget pathway [13] could help explain the similarity of overlap in the midget and parasol populations.

Signal redundancy in parallel visual pathways

Previous work presents a complex picture of RF overlap and signal redundancy in different RGC types. The first direct measurement of RF overlap revealed striking homogeneity among several RGC types in the rabbit retina [16], and provided a theoretical suggestion that this degree of overlap could be optimal for many RGC types (see also [4]). However, several subsequent studies questioned this conclusion by demonstrating that RF overlap varies significantly across different cell types. One study [43] showed that the densest cell type of the rabbit retina exhibits much higher RF overlap than originally reported [16]. Another recent study in primate retina showed that ON parasol cells have slightly higher RF overlap than small bistratified cells [20], which exhibit a distinctive bistratified dendritic morphology and color-opponent light responses. In the larval tiger salamander, RF overlap seems to vary for different RGC types [41], though cell type classification in this species is less certain. Theoretical work has also suggested that the optimal degree of RF overlap can

depend on factors unique to each cell type [44, 45]. Finally, no previous studies have systematically characterized the shape of center and surround profiles in simultaneously recorded populations of RGCs.

While the present results do not provide a unified view of how or why signal redundancy varies across cell types, they unambiguously demonstrate nearly identical redundancy in the dominant visual pathways of primate retina, both in the center and surround of the RF. This result is somewhat surprising in light of the distinct functional roles of the two pathways. Neurons in the magnocellular and parvocellular layers of the lateral geniculate nucleus (LGN), which receive predominantly parasol and midget inputs, respectively [28, 35, 36, 12], exhibit very different projections to visual cortex and systematically different response properties (see [31, 6]). The visual signals carried by these two pathways are thought to mediate largely distinct visual functions, such as perception of change and motion, or fine spatial detail and color, respectively [30]. The unique functions of these pathways begin to emerge in the distinct light response properties of midget and parasol cells [9, 23, 27, 26, 2, 15, 42]. In principle, the different functions of the magnocellular and parvocellular pathways could demand different degrees of signal redundancy in the underlying RGC signals. Instead, the striking similarity suggests that the two high-density pathways may share a common functional requirement – such as the need to efficiently encode visual information in a limited number of optic nerve fibers – and that the observed redundancy may optimally satisfy this requirement.

Future

An important caveat to the present findings is that RF overlap could vary with light level. All the present data were gathered at low photopic light levels (cone-dominated signaling). Different results could hold at scotopic light levels (rod-dominated signaling) [1], because of the distinct circuitry that conveys rod signals to RGCs [24] (see [3]), and because of the distinct functional requirements in conditions where the visual signal is limited by quantum fluctuations in photon absorption (see [19]).

A perplexing problem is how developmental mechanisms produce homogeneous functional organization in the parasol and midget cells despite their structural differences. Clearly, the mechanisms responsible for dendrite growth must operate differently in the two populations. The fact that these mechanisms are precisely counterbalanced with other elements of retinal circuitry, producing nearly identical RF overlap and profiles, suggests that development of RGC mosaics may be governed by the functional outcome, and thus may rely partly on visual experience [17, 47, 22].

Acknowledgments

This work was supported by NIH NRSA and Chapman Foundation (J.G.), the Helen Hay Whitney Foundation (G.D.F.), Burroughs Wellcome Fund Career Award at Scientific Interface (A.S.), DAAD & DFG (M.G.), NSF IGERT DGE-033451 (J.S.), McKnight Foundation (A.M.L. & E.J.C.), NSF Grant PHY-0417175 (A.M.L.), and NIH Grant EY017992 (E.J.C.). We thank C. Hulse for technical assistance; M.I. Grivich, D. Petrusca, W. Dabrowski, A. Grillo, P. Grybos, P. Hottowy, and S. Kachiguine for technical development; H. Fox, M. Taffe, and E. Callaway and K. Osborn for providing access to retinas; S. Barry for machining. This research was supported in part by the National Science Foundation through TeraGrid resources provided by the San Diego Supercomputer Center.

References

1. Barlow HB, Fitzhugh R, Kuffler SW. Change of organization in the receptive fields of the cat’s retina during dark adaptation. J Physiol. 1957; 137(3):338–354. [PubMed: 13463771]
2. Benardete EA, Kaplan E, Knight BW. Contrast gain control in the primate retina: P cells are not x-like, some m cells are. Vis Neurosci. 1992; 8(5):483–486. [PubMed: 1586649]

3. Bloomfield SA, Dacheux RF. Rod vision: pathways and processing in the mammalian retina. Prog Retin Eye Res. 2001; 20(3):351–384. [PubMed: 11286897]
4. Borghuis BG, Ratliff CP, Smith RG, Sterling P, Balasubramanian V. Design of a neuronal array. J Neurosci. 2008; 28(12):3178–3189. [PubMed: 18354021]
5. Brown SP, He S, Masland RH. Receptive field microstructure and dendritic geometry of retinal ganglion cells. Neuron. 2000; 27(2):371–383. [PubMed: 10985356]
6. Callaway EM. Structure and function of parallel pathways in the primate early visual system. J Physiol. 2005; 566(Pt 1):13–19. [PubMed: 15905213]
7. Chichilnisky EJ. A simple white noise analysis of neuronal light responses. Network: Computation in Neural Systems. 2001; 12(2):199–213.
8. Chichilnisky EJ, Kalmar RS. Functional asymmetries in on and off ganglion cells of primate retina. J Neurosci. 2002; 22(7):2737–2747. [PubMed: 11923439]
9. Croner LJ, Kaplan E. Receptive fields of p and m ganglion cells across the primate retina. Vision Res. 1995; 35(1):7–24. [PubMed: 7839612]
10. Dacey DM. The mosaic of midget ganglion cells in the human retina. J Neurosci. 1993; 13(12): 5334–5355. [PubMed: 8254378]
11. Dacey, DM. Origins of perception: retinal ganglion cell diversity and the creation of parallel visual pathways. In: Gazzaniga, MS., editor. The Cognitive Neurosciences. MIT Press; 2004. p. 281-301.
12. Dacey DM, Brace S. A coupled network for parasol but not midget ganglion cells in the primate retina. Vis Neurosci. 1992; 9(3–4):279–290. [PubMed: 1390387]
13. Dacey DM, Packer OS, Diller L, Brainard D, Peterson B, Lee B. Center surround receptive field structure of cone bipolar cells in primate retina. Vision Res. 2000; 40(14):1801–1811. [PubMed: 10837827]
14. Dacey DM, Petersen MR. Dendritic field size and morphology of midget and parasol ganglion cells of the human retina. Proc Natl Acad Sci U S A. 1992; 89(20):9666–9670. [PubMed: 1409680]
15. De Monasterio FM, Gouras P. Functional properties of ganglion cells of the rhesus monkey retina. J Physiol. 1975; 251(1):167–195. [PubMed: 810576]
16. DeVries SH, Baylor DA. Mosaic arrangement of ganglion cell receptive fields in rabbit retina. J Neurophysiol. 1997; 78(4):2048–2060. [PubMed: 9325372]
17. Feller MB, Scanziani M. A precritical period for plasticity in visual cortex. Curr Opin Neurobiol. 2005; 15(1):94–100. 10. [PubMed: 15721750]
18. Field GD, Chichilnisky EJ. Information processing in the primate retina: circuitry and coding. Annu Rev Neurosci. 2007; 30:1–30. [PubMed: 17335403]
19. Field GD, Sampath AP, Rieke F. Retinal processing near absolute threshold: from behavior to mechanism. Ann Revs Physiol. 2005; 67
20. Field GD, Sher A, Gauthier JL, Greschner M, Shlens J, Litke AM, Chichilnisky EJ. Spatial properties and functional organization of small bistratified ganglion cells in primate retina. J Neurosci. 2007; 27(48):13261–13272. [PubMed: 18045920]
21. Frechette ES, Sher A, Grivich MI, Petrusca D, Litke AM, Chichilnisky EJ. Fidelity of the ensemble code for visual motion in primate retina. J Neurophysiol. 2005; 94(1):119–135. [PubMed: 15625091]
22. Hooks BM, Chen C. Critical periods in the visual system: changing views for a model of experience-dependent plasticity. Neuron. 2007; 56(2):312–326. [PubMed: 17964248]
23. Kaplan E, Shapley RM. The primate retina contains two types of ganglion cells, with high and low contrast sensitivity. Proc Natl Acad Sci U S A. 1986; 83(8):2755–2757. [PubMed: 3458235]
24. Kolb H, Famiglietti EV. Rod and cone pathways in the inner plexiform layer of cat retina. Science. 1974; 186(4158):47–49. [PubMed: 4417736]
25. Lee BB. Receptive field structure in the primate retina. Vision Res. 1996; 36(5):631–644. [PubMed: 8762295]
26. Lee BB, Martin PR, Valberg A. Amplitude and phase of responses of macaque retinal ganglion cells to flickering stimuli. J Physiol. 1989; 414:245–263. [PubMed: 2607431]

27. Lee BB, Martin PR, Valberg A. Sensitivity of macaque retinal ganglion cells to chromatic and luminance flicker. J Physiol. 1989; 414:223–243. [PubMed: 2607430]
28. Leventhal AG, Rodieck RW, Dreher B. Retinal ganglion cell classes in the old world monkey: morphology and central projections. Science. 1981; 213(4512):1139–1142. [PubMed: 7268423]
29. Litke AM, Bezayiff N, Chichilnisky EJ, Cunningham W, Dabrowski W, Grillo AA, Grivich M, Grybos P, Hottowy P, Kachiguine S, Kalmar RS, Mathieson K, Petrusca D, Rahman M, Sher A. What does the eye tell the brain? development of a system for the large scale recording of retinal output activity. IEEE Trans Nucl Sci. 2004:1434–1440.
30. Livingstone MS, Hubel DH. Segregation of form, color, movement, and depth: anatomy, physiology, and perception. Science. 1988; 240(4853):740–749. [PubMed: 3283936]
31. Merigan WH, Maunsell JH. How parallel are the primate visual pathways? Annu Rev Neurosci. 1993; 16:369–402. [PubMed: 8460898]
32. Peichl L, Wassle H. Size, scatter and coverage of ganglion cell receptive field centres in the cat retina. J Physiol. 1979; 291:117–141. [PubMed: 480198]
33. Peichl L, Wassle H. Morphological identification of on- and off-centre brisk transient (y) cells in the cat retina. Proc R Soc Lond B Biol Sci. 1981; 212(1187):139–153. [PubMed: 6166011]
34. Peichl L, Wassle H. The structural correlate of the receptive field centre of alpha ganglion cells in the cat retina. J Physiol. 1983; 341:309–324. 11. [PubMed: 6620182]
35. Perry VH, Cowey A. The morphological correlates of x- and y-like retinal ganglion cells in the retina of monkeys. Exp Brain Res. 1981; 43(2):226–228. [PubMed: 7250268]
36. Perry VH, Oehler R, Cowey A. Retinal ganglion cells that project to the dorsal lateral geniculate nucleus in the macaque monkey. Neuroscience. 1984; 12(4):1101–1123. [PubMed: 6483193]
37. Polyak, SL. The retina. University of Chicago Press; Chicago: 1941.
38. Puchalla JL, Schneidman E, Harris RA, Berry MJ. Redundancy in the population code of the retina. Neuron. 2005; 46(3):493–504. [PubMed: 15882648]
39. Rieke, F.; Warland, D.; de Ruyter van Steveninck, RR.; Bialek, W. Spikes: exploring the neural code. MIT Press; Cambridge, MA: 1997.
40. Rodieck RW. Quantitative analysis of cat retinal ganglion cell response to visual stimuli. Vision Res. 1965; 5(11):583–601. [PubMed: 5862581]
41. Segev R, Puchalla J, Berry MJ 2nd. Functional organization of ganglion cells in the salamander retina. J Neurophysiol. 2006; 95(4):2277–2292. [PubMed: 16306176]
42. Troy JB, Lee BB. Steady discharges of macaque retinal ganglion cells. Visual Neuroscience. 1994; 11(1):111–118. [PubMed: 8011574]
43. van Wyk M, Taylor WR, Vaney DI. Local edge detectors: a substrate for fine spatial vision at low temporal frequencies in rabbit retina. J Neurosci. 2006; 26(51):13250–13263. [PubMed: 17182775]
44. Vincent BT, Baddeley RJ. Synaptic energy efficiency in retinal processing. Vision Res. 2003; 43(11):1283–1290. [PubMed: 12726834]
45. Vincent BT, Baddeley RJ, Troscianko T, Gilchrist ID. Is the early visual system optimised to be energy efficient? Network. 2005; 16(2–3):175–190. [PubMed: 16411495]
46. Watanabe M, Rodieck RW. Parasol and midget ganglion cells of the primate retina. J Comp Neurol. 1989; 289(3):434–454. [PubMed: 2808778]
47. White LE, Fitzpatrick D. Vision and cortical map development. Neuron. 2007; 56(2):327–338. [PubMed: 17964249]
48. Yamada ES, Bordt AS, Marshak DW. Wide-field ganglion cells in macaque retinas. Vis Neurosci. 2005; 22(4):383–393. [PubMed: 16212697]
49. Yang G, Masland RH. Receptive fields and dendritic structure of directionally selective retinal ganglion cells. J Neurosci. 1994; 14(9):5267–5280. [PubMed: 8083735]

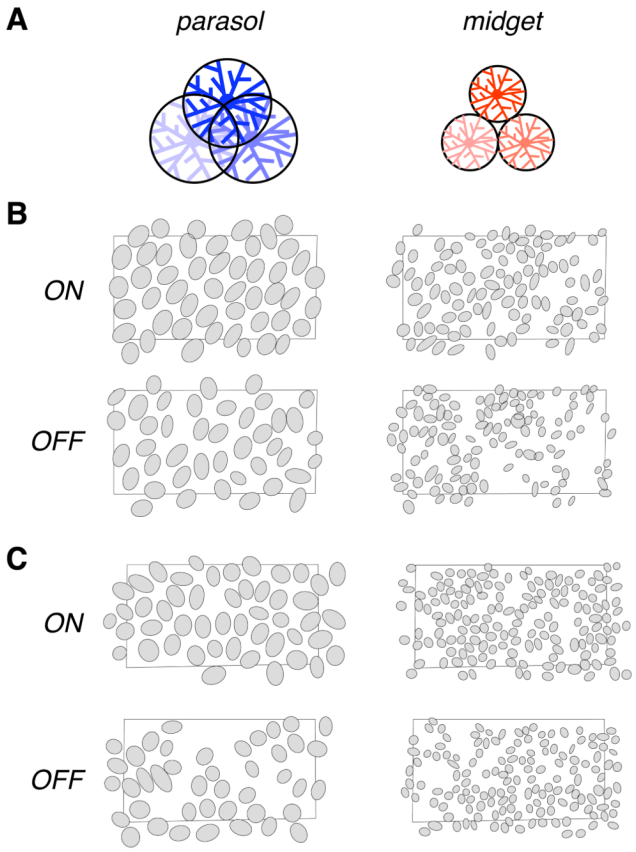

Figure 1.

Parasol and midget RF mosaics and anatomical prediction. **A.** Previous anatomical findings indicate that parasol cell dendritic fields overlap substantially, with the tips of each dendritic field reaching the soma of its neighbors in the mosaic, while midget cell dendritic fields abut at their boundaries. **B.** Each panel shows the RFs of simultaneously recorded ON and OFF parasol and midget cells from one retina, with each RF represented as the 1 standard deviation boundary of a Gaussian fit to the RF center. Black rectangles indicate the outline of recording array (1800 by 900 micrometers). Gaps in the mosaic probably represent unrecorded cells. Retinal temporal equivalent eccentricity: 6.4 mm. **C.** Same as in B for a second preparation (temporal equivalent eccentricity 9.0 mm).

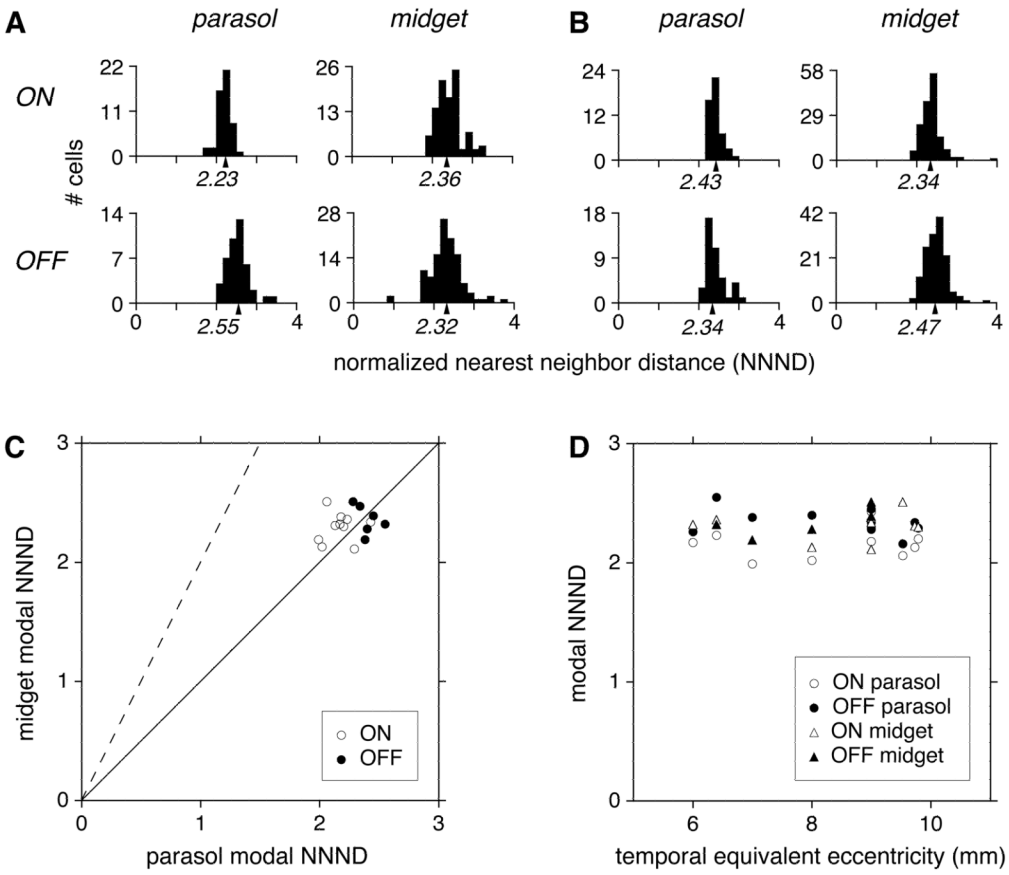

Figure 2.

Quantitative analysis of RF overlap. The normalized nearest neighbor distance (NNND) measures RF spacing relative to RF size; if two mosaics have the same degree of RF overlap, they will have the same NNND. **A.** NNND values for the mosaics of parasol and midget cells shown in Figure 1B, with the modal NNND (mean of the densest 75% of values) indicated on the abscissa. Because the recordings did not sample every cell in the mosaic, the modal NNND was computed in a way that excluded outlying points, and the robustness of this calculation was confirmed by subsampling analysis (see Methods). **B.** Similar data, for the preparation in Figure 1C. **C.** Data summarizing the RF overlap of 36 mosaics (3,221 cells spanning 10 preparations). Modal NNND values of simultaneously recorded parasol and midget mosaics are compared separately for ON cells (open circles) and OFF cells (filled circles). Solid line indicates equality, dashed line indicates the prediction from anatomical findings that NNND should be twice as large for midget cells. **D.** NNND values as a function of retinal eccentricity, for ON (open) and OFF (filled) cells of both midget (triangle) and parasol (circle) types.

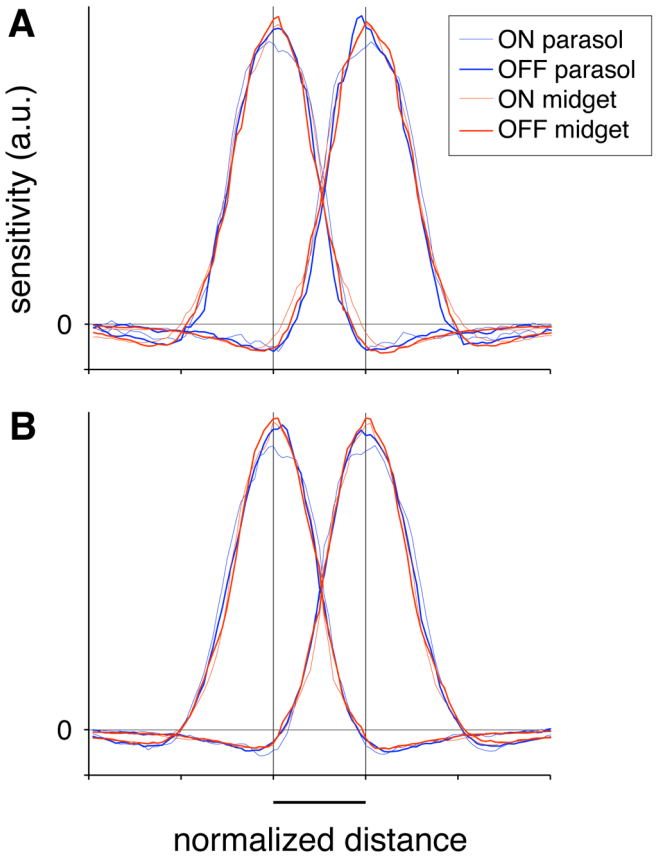

Figure 3.

Nearest neighbor RF profiles for ON and OFF parasol and midget cells. **A.** For each cell type, the average RF profiles of a cell and its nearest neighbor were computed directly by interpolation of the spatial receptive field (see Methods). Distance and amplitude were normalized to focus on the RF profile shape independently of absolute size, spacing, and sensitivity. Distance was normalized for each pair of nearest neighbors (see Methods), and the scale bar at bottom indicates the distance between nearest neighbors. Sensitivity was normalized to have the same variance across cell types (see Methods). Data are from the preparation shown in Figure 1C. **B.** Same as A, from a second preparation (temporal equivalent eccentricity 9 mm).